Appl. Phys. B (2013) 110:101–110
DOI 10.1007/s00340-012-5256-6

Applied Physics B
Lasers and Optics

Multi-phonon-assisted relaxation and Yb^{3+} sensitized bright red-dominant upconversion luminescence of Ho^{3+} in YF_3-BaF_2-$Ba(PO_3)_2$ glass

Boyuan Lai · Li Feng · Jianhui Zhang · Jing Wang · Qiang Su

Received: 7 January 2010 / Revised: 11 August 2012 / Published online: 24 November 2012

Abstract Unusual bright red-dominant upconversion light was observed in Ho^{3+}/Yb^{3+} co-doped YF_3-BaF_2-$Ba(PO_3)_2$ glasses excited by the 980-nm laser diode at room temperature. The integral intensity ratios of the red upconversion emission to the green one reached about 10:1 in optimized $0.125Ho^{3+}$-$15Yb^{3+}$ co-doped sample. In order to find out its behind-the-scene mechanism, the optical properties and the phonon-assisted relaxations on the excited levels of Ho^{3+} in our samples were investigated. Additionally, the effects of the concentrations of the doping ions, excitation pump power, and temperature on the upconversion emissions were also systematically studied. These results revealed that the proper phonon frequency of fluorophosphate glasses, the efficient phonon-assisted relaxations from $^5I_6$ to $^5I_7$ levels (4,960 s^{-1}), and the long lifetime of the $^5I_7$ (about 2.8 ms) levels should be responsible for bright red upconversion emission at a much greater concentration ratio of C^{3+}_{Yb}/C^{3+}_{Ho}.

B. Lai · J. Zhang · J. Wang (✉) · Q. Su
Ministry of Education Key Laboratory of Bioinorganic and Synthetic Chemistry, State Key Laboratory of Optoelectronic Materials and Technologies, School of Chemistry and Chemical Engineering, Sun Yat-Sen University, Guangzhou 510275, People's Republic of China
e-mail: ceswj@mail.sysu.edu.cn

Q. Su
e-mail: suqiang@mail.sysu.edu.cn

L. Feng
Institute of Materials Science and Engineering, Shijiazhuang University of Economics, Shijiazhuang 050031, People's Republic of China

1 Introduction

In recent years, a number of studies have been carried out to develop rare-earth (RE) ion-doped materials capable of efficient frequency upconversion and to utilize these materials as compact solid-state lasers, biomedical diagnostic labels [1, 2], temperature sensors [3], and clean energy and color display phosphors [4]. Among the RE ions, Ho^{3+}, Er^{3+}, and Tm^{3+} were the most attractive active ions applied to infrared-to-visible upconversion fluorescence due to their favorable energy-level structures. In addition, upconversion florescence of these ions has been extensively investigated in a variety of crystalline and vitreous materials. Low-cost fluorophosphates glasses were expected to be promising and applicable hosts for the upconversion florescence of RE^{3+} ions because of their low melting temperature, good homogeneity, improved chemical/physical stability, and flexible optical properties [5]. On the other hand, with the commercialization of the ~980-nm laser diode (LD), Yb^{3+} has become a popular sensitizer for $Ho^{3+}/Er^{3+}/Tm^{3+}$ ion to increase the optical pumping efficiency due to its larger absorption cross-section and efficient energy transfer from Yb^{3+} ions to the active ions.

Under the near-infrared excitations, bright blue- or green-upconversion light was usually dominating in most RE^{3+} single- or multi-doped materials. Red upconversion emission (~650 nm) can be theoretically generated by the $^4F_{9/2} \rightarrow {}^4I_{15/2}$ radiative transition of Er^{3+}, $^5F_5 \rightarrow {}^5I_8$ of Ho^{3+}, and $^1G_4 \rightarrow {}^3F_4$ of Tm^{3+}. However, red upconversion emission was not so strong when compared with the green ones of Er^{3+} ($^2H_{11/2}$, $^4S_{3/2} \rightarrow {}^4I_{15/2}$) and Ho^{3+} ($^5F_4$, $^5S_2 \rightarrow {}^5I_8$), and the blue one of Tm^{3+} ($^1G_4 \rightarrow {}^3H_6$). Therefore, bright red-dominant upconversion light was only reported in a few literatures [6–10]. In these cases, red upconversion light was usually caused by the relatively high

concentration Ho^{3+} that leads to the cross-relaxations among different levels of Ho^{3+} and therefore inhibits green upconversion emission [8–10]. Here we will report a red-dominant upconversion light in YF_3-BaF_2-$Ba(PO_3)_2$ glasses where the intensity ratios of the red emission to the green one were greater than 9:1, even when the concentration ratios of C_{Yb}^{3+}/C_{Ho}^{3+} were great as 600:1. In order to investigate this unusual red-dominant light in the present case, the structures of the glasses were evaluated to determine the cut-off frequency of phonons through IR or Raman spectra. The radiative transitions probabilities and the relaxation rates of Ho^{3+} were calculated through using the Judd–Ofelt theory. The temperature effect on the decay time of the green down-conversion emission of Ho^{3+} was studied to investigate the efficient phonon-assisted relaxation in the glass. The effects of excitation pump power, the concentration of doping ions, and temperature were also studied.

2 Experimental

The composition of samples used in this paper can be expressed as (in mol %) follows:

$$(40-x-y)YF_3-22Ba(PO_3)_2-38BaF_2:xHoF_3-yYbF_3,\ \text{abbreviated as YBPF}:x\text{Ho}-y\text{Yb, and } 40AlF_3-22Ba(PO_3)_2-38BaF_2,\ \text{as ABPF,}$$

where $x = 0.05$, 0.075, 0.1, 0.125, 0.2, 0.25, 0.3, 1.0, and $y = 0$, 5, 10, 15, 20, 25, 30. Starting powders were thoroughly ground with agate mortar and pestle, kept at 450 °C for 1 h for the pre-reaction, and then melted at 1,050–1,150 °C for 15 min in a corundum crucible in ambient atmosphere. The melts were poured on a preheated stainless steel plate and then annealed to room temperature. The obtained glasses were cut and polished into 2-mm thick slabs for optical property measurements.

Density was measured according to Archimedes' principle using distilled water as the immersion liquid. Refractive index was measured on an Abbe refractometer using monobromonaphthalene as adhesive coating. The density and refractive index of YBPF: 1Ho-0Yb sample were determined to be 4.602 g/cm^3 and 1.593, respectively. The infrared (IR) absorption spectra of YBPF: 0Ho-0Yb and ABPF glass were measured on a Nicolet/Nexus 670 FT-IR Analyzer using KBr pellets in 1,500–500 cm^{-1} range. The Raman spectrum in the 300–3,000 cm^{-1} range was obtained using a Renishaw inVia Microscope with a 514-nm laser excitation.

UV/Vis/NIR Absorption spectrum of YBPF: 1Ho-0Yb in 30,000–5,000 cm^{-1} range was recorded by a Varian Cary 5000 UV/Vis/NIR spectrophotometer at the scan step of 10 cm^{-1}. Visible up- and down-conversion signals were recorded by an Edinburgh FSP920 Combined Time Resolved and Steady State Fluorescence Spectrometer equipped with thermo-electric cooled red-sensitive PMT. A 450-W Xe900 steady-state xenon lamp (ozone free) and a μF920H flash lamp were used as the excitation sources in steady and dynamic down-conversion luminescence measurement, respectively. The pulse repetition rate of μF920H was 100 Hz and the pulse width was about 1.5–3.0 μs. A ~980-nm centered continue wave (CW) LD with a maximum power of 1 W was used for the excitation source for upconversion luminescence. For the temperature-dependent measurement, the sample was mounted in a 77- to 500-K Oxford Optistat DN-V liquid nitrogen optical cryostat with an ITC601 temperature controller.

3 Results and discussions

3.1 IR and Raman spectra of YBPF glasses

The IR spectrum of the YBPF: 0Ho-0Yb glasses is shown in Fig. 1a and that of ABPF glasses is also presented in for comparison, since the glass-forming ability of Y^{3+} is similar to that of Al^{3+} [5], and the structures of Al^{3+}-base (AlF_3 and/or $Al(PO_3)_3$) fluorophosphate glasses have been investigated more frequently. According to previous studies[11–13], for fluorophosphates glasses containing 10–25 mol % $(PO)_3^-$, the broad band ranging from 800 to 1,400 cm^{-1} can be ascribed to the stretching and asymmetric vibrations of P–O–P, O–P–O, F–P–F, and/or O–P–F bonds, and the broad band ranging from 500 to 700 cm^{-1} can be ascribed to the non-bridging bond in $M[O]_{4,6}$, $M[F]_{4,6}$ and/or $M[O,F]_6$ anion units (M = Al^{3+} or RE^{3+}). The ~735-cm^{-1} band can be ascribed to P–O–P stretching vibration [11, 12], but it may be also ascribed to the non-bridging band in anion units $M[O]_4$ and $M[O,F]_4$ [13]. Due to the larger radius, RE^{3+} ions incline to form anion units $RE[O]_6$, $RE[F]_6$, and/or $RE[O,F]_6$. And this will break the F–P–F long chain in the glasses, then -P- connect to -O- to form PO_2^-/PO_3^- units. So, for YBPF samples, their ~910 and 735 cm^{-1} bands ($(P–O–P)_{as}$, and $(P–O–P)_{ss}$) are more distinct when compared with the ABPF glasses.

Raman spectra of YBPF: 0Ho-0Yb glass are shown in Fig. 1b and six bands are labeled as *a–f*. According to previous literatures [11, 14, 15], band *a* centered at 340 cm^{-1} may relate to the overlapping vibration of the skeletal deformation vibration of metaphosphate chains and PO_2 deformation vibration of pyrophosphate segments. Broadband *b* from 400 to 690 cm^{-1} and the band *c* centered at 745 cm^{-1} are ascribed, respectively, to the group vibration of anion units $RE[F]_6/RE[O,F]_6$ and the stretching vibration of P–O–P, consisting of the IR spectra. Band *d* can be ascribed to the P–F vibration in $PO_2F_2^-$ unit. The strong band

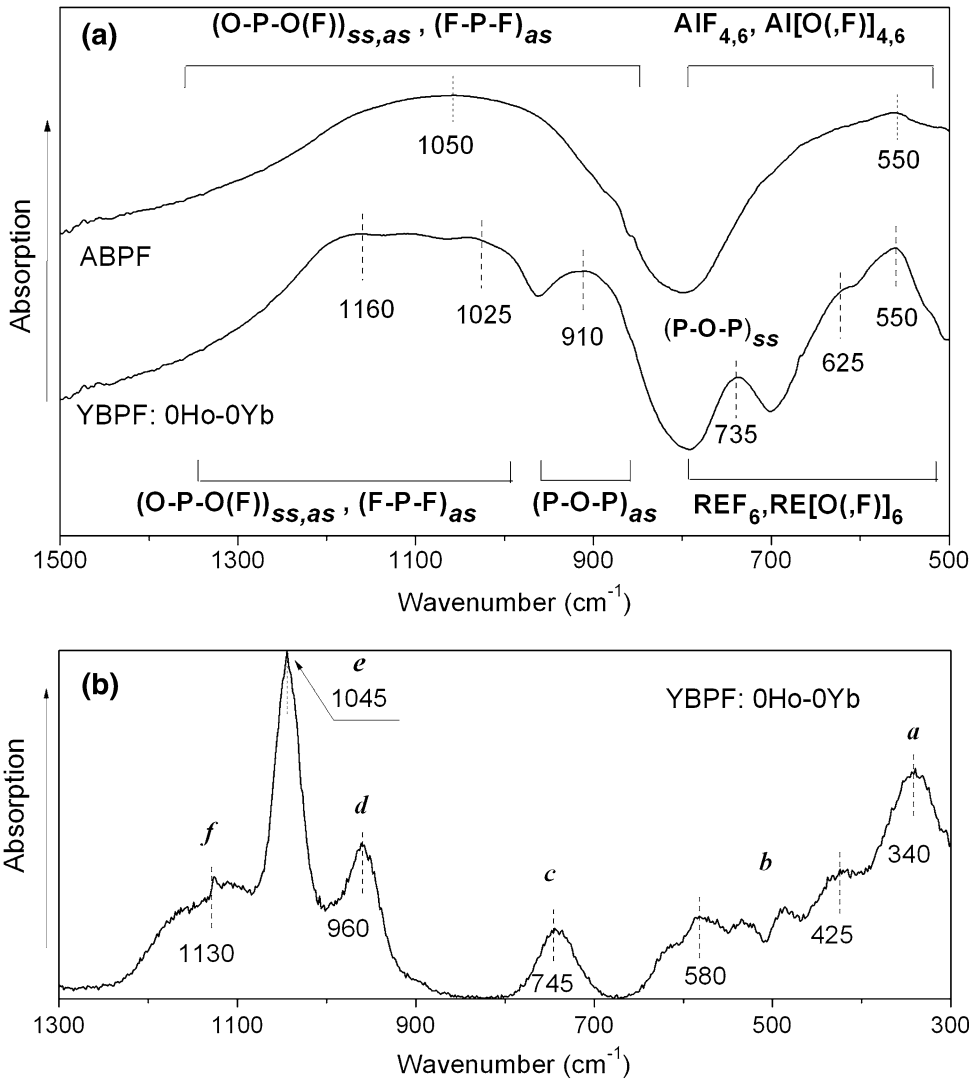

Fig. 1 **a** IR absorption spectra of YBPF: 0Ho-0Yb glass and ABPF glass. **b** Raman spectra of YBPF: 0Ho-0Yb glass

e at 1,045 cm^{-1} can be ascribed to the symmetry stretching vibration of O–P–O(F) in $P_2(O,F)_7$ dimer, since the F^-/PO_3^- reaches about 9:2 in our sample. And the shoulder band *f* around 1,130 cm^{-1} is related to the vibration of O–P–O in metaphosphate tetrahedron.

3.2 UV–Vis–NIR absorption and Judd–Ofelt calculation

The room temperature UV–Vis–NIR absorption spectrum of YBPF: 1Ho-0Yb glass ($l = 2.42$ mm) is shown in Fig. 2. The absorption bands are attributed to $f \rightarrow f$ transitions from the ground state $^5I_8$ to the different excited states [16]. The experimental oscillator strengths of these transitions are calculated from

$$P_{\exp} = \frac{mc^2}{e^2\pi N}\int \frac{2.303}{l}\cdot \mathrm{OD}(v)\mathrm{d}v, \quad (1)$$

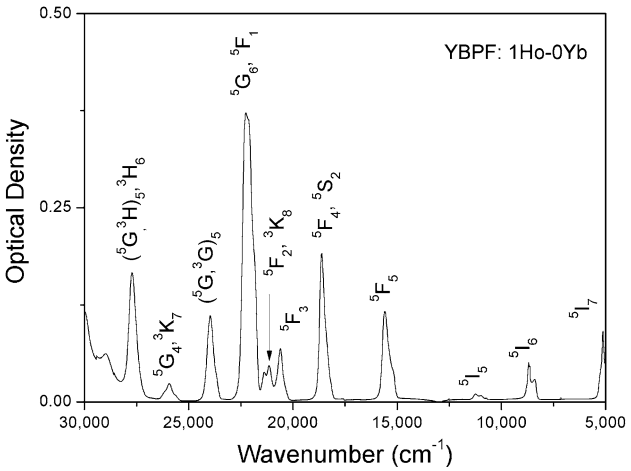

Fig. 2 UV–Vis-NIR Absorption spectrum of YBPF: 1Ho-0Yb glass at room temperature

where *m* and *e* are the electron mass and charge, respectively, *c* is the speed of light, *l* is the thickness of sample, *N* is the

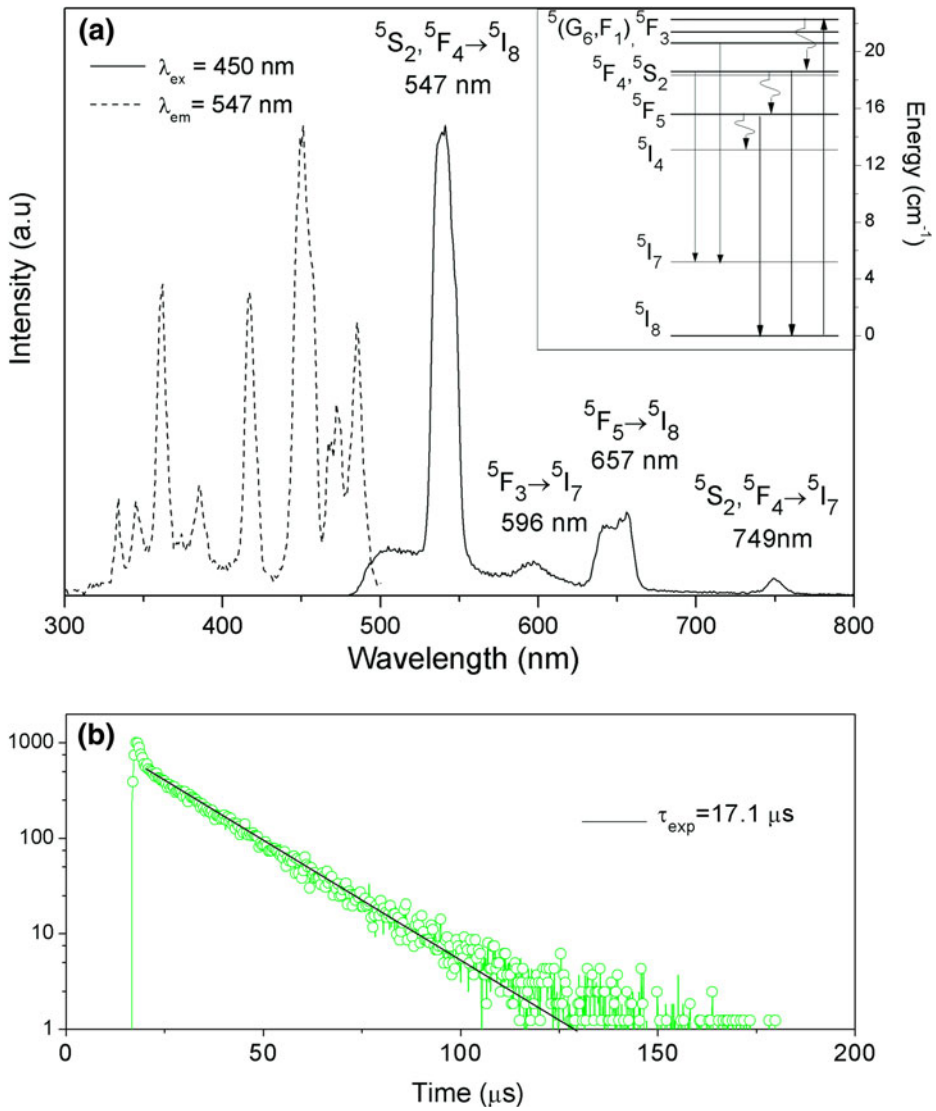

Fig. 3 **a** Excitation spectra (*dot line*) and emission spectra (*solid line*) of YBPF: 0.05Ho-0Yb at room temperature in down-conversion case (Inset: simplified energy-level diagram of Ho^{3+}, *wavy arrows* denote non-radiative relaxation). **b** Decay curve of the 547 nm emission ($\lambda_{ex} = 450$ nm)

number of absorbing ions in the unit volume, v is the wave number, and $OD(v)$ is the optical density. By a least square fitting of the experimental and theoretical oscillator strengths, the Judd–Ofelt parameters are obtained: $\Omega_2 = 2.95 \times 10^{20}$, $\Omega_4 = 2.61 \times 10^{20}$ and $\Omega_6 = 2.15 \times 10^{20}\,cm^{-2}$, respectively.

These J–O parameters are important for the investigation of the local structure and bonding in the vicinity of RE ions. Previous works [17–19] reveal that the Ω_2 is sensitive to symmetry of the RE ions site and the covalence between RE ions and ligand ions, and the Ω_6 is affected by the electronic density of RE^{3+} [20, 21]. For comparison, the $\Omega_{2,4,6}$ of Ho^{3+} obtained from YBPF: 1Ho-0Yb and some other hosts are tabulated in Table 1. It can be seen that the Ω_2 of our glass as well as other glasses are larger than that of crystalline materials, mainly attributed to its lower symmetry. Among glasses, Ω_2 of our glass is smaller than that of pure oxide glass but larger than that of pure fluoride glass, since the covalence of Ho–O band becomes weak due to the strong attraction of F^- ions for the electrons of Ho^{3+}. On the other hand, the attraction of F^- also decreases the shielding effect of 6*s* electrons of Ho^{3+} on the 5*d* ones, and thus increases the electronic density of the 5*d* orbit, resulting in an increment on the value of Ω_6. Furthermore, in fluorophosphate glasses, π-electron

Table 1 Comparisons of experimental intensity parameters Ω_λ of YBPF: 1Ho-0Yb glass with other samples

Host compositions	Ω_2 ($\times 10^{-20}$)	Ω_4	Ω_6	Reference
HoP_5O_{14} crystal	1.45	1.40	1.46	[22]
LaF_3 crystal	1.16	1.38	0.88	[6]
Al_2O_3-BaO-MgO-K_2O -P_2O_5	3.33	3.01	0.61	[23]
ZrF_4-LaF_3-AlF_3-BaF_2	2.28	2.08	1.73	[24]
CaF_2-$NaPO_3$	3.23	2.71	1.82	[25]
YF_3-BaF_2-$Ba(PO_3)_2$	2.95	2.61	2.15	This work

donation of non-bridging P–O bond [21] to the 5*d* orbital of Ho^{3+} also greatly augments the Ω_6.

On the other hand, with the experimental intensity parameters $\Omega_{2,\ 4,\ 6}$, the spontaneous radiative transition probabilities from an initial manifold $|(S', L')J'\rangle$ to a final manifold $\left|(\overline{S}, \overline{L})\overline{J}\right\rangle$can be calculated from:

$$\begin{aligned} A_{\mathrm{ed}}[(S', L')J'; (\overline{S}, \overline{L})\overline{J}] &= A_{\mathrm{ed}} + A_{\mathrm{md}} \\ &= \frac{64\pi^4 v^3}{3h(2J'+1)} \cdot \frac{n(n^2+2)^2}{9} \\ &\quad \cdot e^2 \sum_{\lambda=2,4,6} \Omega_\lambda \left| \left\langle (S, L)J \left\| U^{(\lambda)} \right\| (S', L')J' \right\rangle \right|^2 \\ &\quad + \frac{64\pi^4 v^3}{3h(2J'+1)} \cdot n^3 \cdot \frac{e^2}{4m^2c^2} \left| \langle (S, L)J \| L + 2S \| (S', L')J' \rangle \right| \end{aligned} \tag{2}$$

where $\left\langle \left\| U^{(\lambda)} \right\| \right\rangle$ are the reduced matrix elements. And then the spontaneous emission life time τ_{rad} of the initial manifold can be yielded as:

$$\tau_{\mathrm{rad}} = \frac{1}{\sum_{\overline{S},\overline{L},\overline{J}} A_{\mathrm{ed}}[(S', L')J'; (\overline{S}, \overline{L})\overline{J}]}. \tag{3}$$

The radiative transition probabilities (A_{ed}, A_{md}) and radiative lifetimes (τ_{rad}) of the $^5I_7$, $^5F_5$, and $^5S_2$,$^5F_4$ levels are listed in Table 2.

Table 2 Radiative transition probabilities A_{rad}, fluorescence branching ratios β and radiative lifetimes τ_{rad} of different excited levels of Ho^{3+} in YBPF glass

Transitions		v (cm^{-1})	A_{ed} (s^{-1})	A_{md} (s^{-1})	A_{rad} (s^{-1})	β	τ_{rad} (μs)
$^5I_7$→	$^5I_8$	5,150	88	24	112	1.00	8928
$^5I_6$→	$^5I_8$	8,690	216		252	0.86	3968
	$^5I_7$	3,540	22	14		0.14	
$^5I_5$→	$^5I_8$	11,240	77		190	0.41	5263
	$^5I_7$	6,090	106			0.56	
	$^5I_6$	2,550	7			0.03	
$^5F_5$→	$^5I_8$	15,590	3,332		3,958	0.84	253
	$^5I_7$	10,440	498			0.13	
	$^5I_6$	6,900	120			0.03	
	$^5I_5$	4,350	8			0.00	
$^5F_4$→	$^5I_8$	18,360	4,036		4,899	0.82	204
	$^5I_7$	13,210	420			0.09	
	$^5I_6$	9,670	269			0.05	
	$^5I_5$	7,120	163			0.03	
	$^5F_5$	2,770	7	4		0.00	
$^5S_2$→	$^5I_8$	18,620	1,651		3,027	0.55	330
	$^5I_7$	13,470	1,128			0.37	
	$^5I_6$	9,930	198			0.06	
	$^5I_5$	7,380	50			0.02	
	$^5F_5$	3,030	1			0.00	

3.3 Phonon-assisted relaxation on excited levels of Ho^{3+} in YBPF glass

Figure 3a presents the visible down-conversion excitation and emission spectra of YBPF: 0.05Ho-0Yb. The strongest excitation band centered at 450 nm can be ascribed to the $^5I_8 \rightarrow {}^5G_6$, $^5F_1$ absorption. The emission bands peaks at 547 and 657 nm are assigned to the $^5F_4$, $^5S_2 \rightarrow {}^5I_8$ and $^5F_5 \rightarrow {}^5I_8$ radiative transitions, and the emission bands centered at 596 and 749 nm can be assigned to $^5F_3 \rightarrow {}^5I_7$ and $^5F_4$, $^5S_2 \rightarrow {}^5I_7$ radiative transitions, respectively. The integral intensity ratio of the red emission to the green one (I_{657nm}/I_{547nm}) is about 0.24. The decay curve of the green emission is depicted in the Fig. 3b. It shows a single-exponential behavior and gives the experimental decay time τ_{exp} of 17.1 μs. In 0.05 % Ho^{3+} singly doped sample, the cross-relaxation among the excited levels can be neglected, and the relaxation rate W_{R} of the $^5F_4$,$^5S_2$, and $^5F_5$ levels can be calculated from

$$W_R = \frac{1}{\tau_{\mathrm{exp}}} - \frac{1}{\tau_{\mathrm{rad}}}. \tag{4}$$

At room temperature, the W_{R} of the $^5S_2$, $^5F_4$ level is 50,553 s^{-1} and it is much greater than the A_{rad} of $^5S_2$, $^5F_4$ level listed in Table 2. This should relate to the high cut-off frequency phonon of the fluorophosphate glasses. As Raman spectra (Fig. 1b) shows, YBPF glasses have the strongest absorption at 1,045 cm^{-1}, which has been ascribed to $O\text{–}P\text{-}O(F)_{SS}$ in $P_2(O,F)_7$ dimer. Meanwhile, the UV–Vis-NIR absorption spectra (Fig. 2) shows that the energy gap between the $^5S_2$, $^5F_4$, and $^5F_5$ levels is about 2,770 cm^{-1}. By coupling with the vibrations in the glass and emitting about three phonons, Ho^{3+} in the $^5S_2$, $^5F_4$ state relaxes fast to $^5F_5$ and then generates red emission. It must be noted that the down-conversion fluorescence is still green-dominant due to the greater A_{ed} of the $^5S_2 + {}^5F_4 \rightarrow {}^5I_8$ radiative transition. Meanwhile, the multi-phonon-assisted relaxation (MPR) on the $^5F_5$ level works also efficiently ($\tau_{\mathrm{exp}} = 19.7$ μs, $W_{\mathrm{R}} =$ 46,805 s^{-1}) and further reduces the red emission intensity [26, 27].

In order to prove the 3-phonon-assisted relaxation on the $^5S_2$, $^5F_4$ level, the temperature effect on the decay time τ_{exp} and multi-phonon-assisted relaxation rate (W_{MPR}) of the $^5S_2$, $^5F_4$ level are investigated as shown in Fig. 4a, b, respectively. As temperature increases from 77 to 490 K, the τ_{exp} decreases from 17.2 to 14.5 μs while the W_{MPR} increases from 50,258 s^{-1} to 61,084 s^{-1}. According to previous works of M. J. Weber and H. W. Moos et al. [28–32], the relation between the W_{MPR} of an excited level and temperature can be written as

$$W_{MPR}(T) = W_R(0)[1 - \exp(-h\omega/kT)]^{-n}, \tag{5}$$

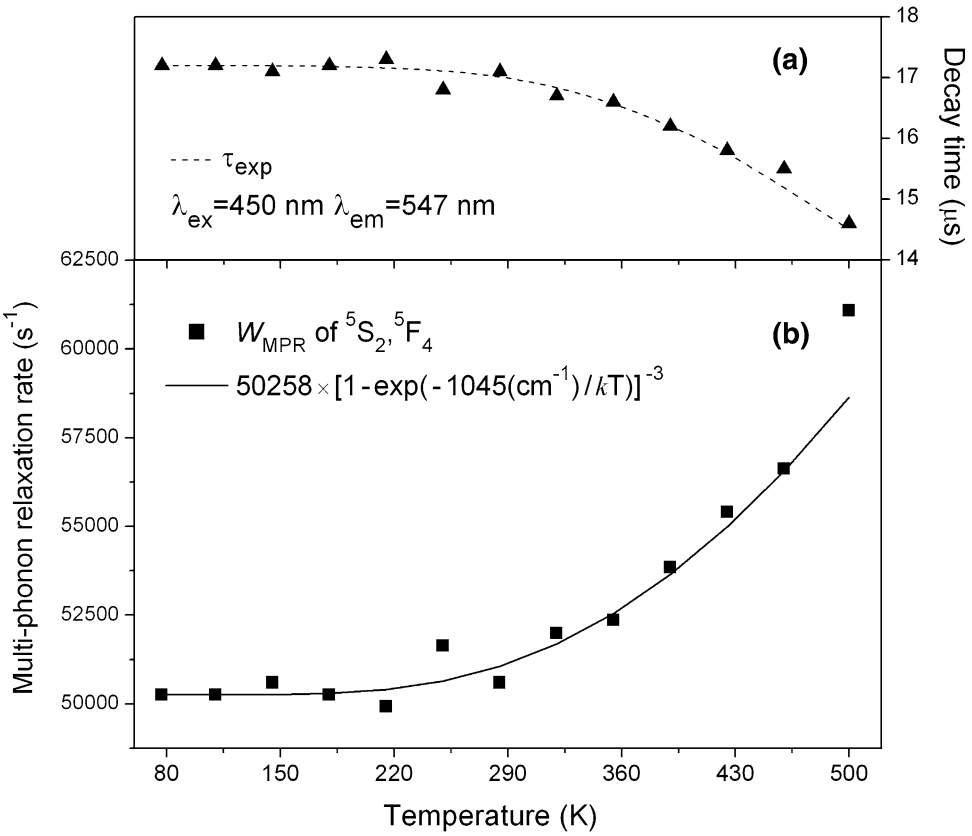

Fig. 4 **a** Temperature dependence of the experimental decay time of the 547 nm down-conversion emission; **b** Temperature dependence of the multi-phonon relaxation rate of the $^5S_2$, $^5F_4$ level. *Solid line* is the temperature-relaxation model obtained from Eq.(5) assuming $h\omega = 1{,}045$ cm^{-1} and $n = 3$

where h is the Planck constant, k is the Boltzmann constant; ΔE is the energy gap to the next-lower level, ω is the cut-off frequency of the phonon, n is the order of the MPR process required to bridge the energy gap, and $n = \Delta E/h\omega$, $W_R(0)$ is the decay rate at 0 K, but here we use the rate at 77 k. For the $^5S_2$, $^5F_4$ level of Ho^{3+} in our sample, Fig. 4b shows the observed data well fit to the model calculated from Eq.(5) by assuming three 1,045 cm^{-1} phonons were engaged.

These phonon-assisted processes are also efficient for the relaxations with the energy gaps wider than 3,000 cm^{-1}. However, when the energy gaps are wider than 5,000 cm^{-1}, the W_{MPR}s of the relaxation become comparably small since five or more phonons are needed to bridge the gaps. The dependence of the relaxation rate W_{MPR} on the energy gap ΔE to the next-lower level can be expressed as [29–31]

$$W_{MPR} = W_0 \cdot \exp(-\alpha \Delta E/h\omega), \quad (6)$$

where the W_0 is the relaxation rate when $\Delta E = 0$, and α is host-dependent constant. The data on the W_{MPR} of some excited levels of Ho^{3+}, Er^{3+}, and Tm^{3+} in YBPF glass at room temperature are plotted semi-logarithmically versus ΔE in Fig. 5, and the α is fitted to be 1.97 and the W_0 to be 3.64×10^6 s^{-1}. This linear plot is helpful to study the relaxations on some levels when the actual lifetimes of these levels cannot be experimentally obtained, such as the $^5I_6$ and $^5I_7$ levels of Ho^{3+} in our case. According to Eqs.(6) and (4), the W_{MPR} of the $^5I_6$ levels is estimated to be close to about 4,600 s^{-1} ($\Delta E = 3{,}540$ cm^{-1}) and thus the level lifetime decreases from 4.0 ms (τ_{rad}) to about ~210 μs, while the W_{MPR} of the $^5I_7$ level ($\Delta E = 5{,}150$ cm^{-1}) is estimated to be about ~220 s^{-1}, and the level lifetime reaches about ~3.0 ms.

3.4 Red-dominant upconversion light of Ho^{3+}/Yb^{3+} co-doped samples

Figure 6a shows the photograph and upconversion emission spectrum of YBPF: 0.125Ho-15Yb excited by a 980-nm CW LD with the pump power (P_{ex}) about 450 mW/mm^2 at room temperature. The green emission band peaking at 542 nm corresponds to the $^5F_4$, $^5S_2 \rightarrow {}^5I_8$ transition and the red emission peaking at 657 nm corresponds to the $^5F_5 \rightarrow {}^5I_8$ transitions. The weak blue broad emission centered at 476 nm is ascribed to the $^5F_3 \rightarrow {}^5I_8$ transition in many previous reports, but here it more probably comes from the cooperative upconversion of Yb^{3+} pairs in $Yb[F]_6/Yb[O,F]_6$ cluster [33] since it is also observed in the samples singly doped with Yb^{3+}. As the

photograph shows, YBPF: 0.125Ho-15Yb gives off bright red-dominant upconversion light, the intensity ratio of I_{657nm}/I_{542nm} reaches 10:1. This red light could be readily seen with the naked eye at pump power as low as 60 mW/mm^2. The effect of concentration of Ho^{3+} and Yb^{3+} on the intensities of upconversion emissions is shown in Fig. 6b, c. Since the concentration of Ho^{3+} is not high enough to induce intense cross-relaxations among different levels of Ho^{3+}, the effects of increasing Ho^{3+} on the emissions intensities are not very notable. On the other hand, due to the strong absorption of Yb^{3+} around 980 nm and the efficient energy transfer from Yb^{3+} to Ho^{3+}, increasing Yb^{3+} concentration benefits the populations on the excited levels of Ho^{3+} and thus greatly enhances the emission intensities before the intense concentration quenching (C^{3+}_{Yb}= 30 mol %). For all the co-doped glasses, the red

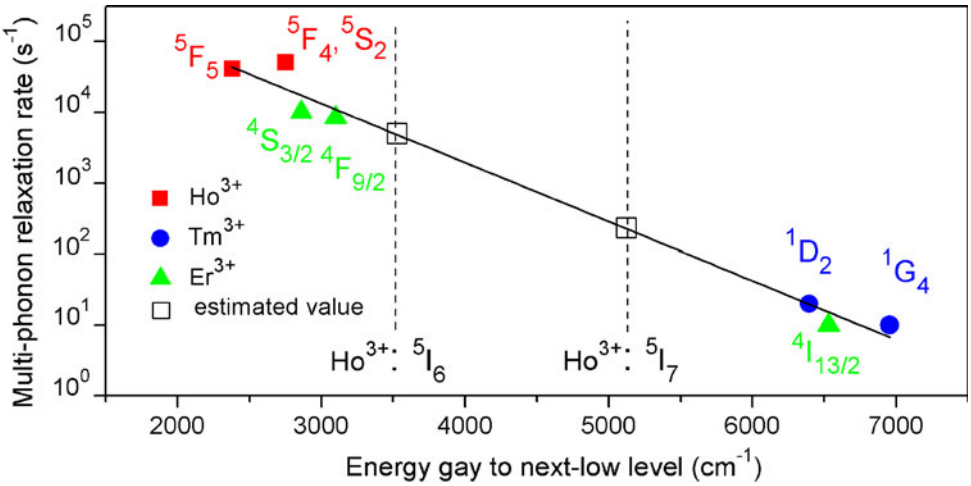

Fig. 5 Dependence of the phonon-assisted relaxation rate on the energy gap between different excited levels of RE^{3+} in YBPF glass at room temperature, and *solid line* is the fitted exponential decay curve (doping concentrations of Ho^{3+} and Tm^{3+} are 0.05 % and that of Er^{3+} is 0.025 %)

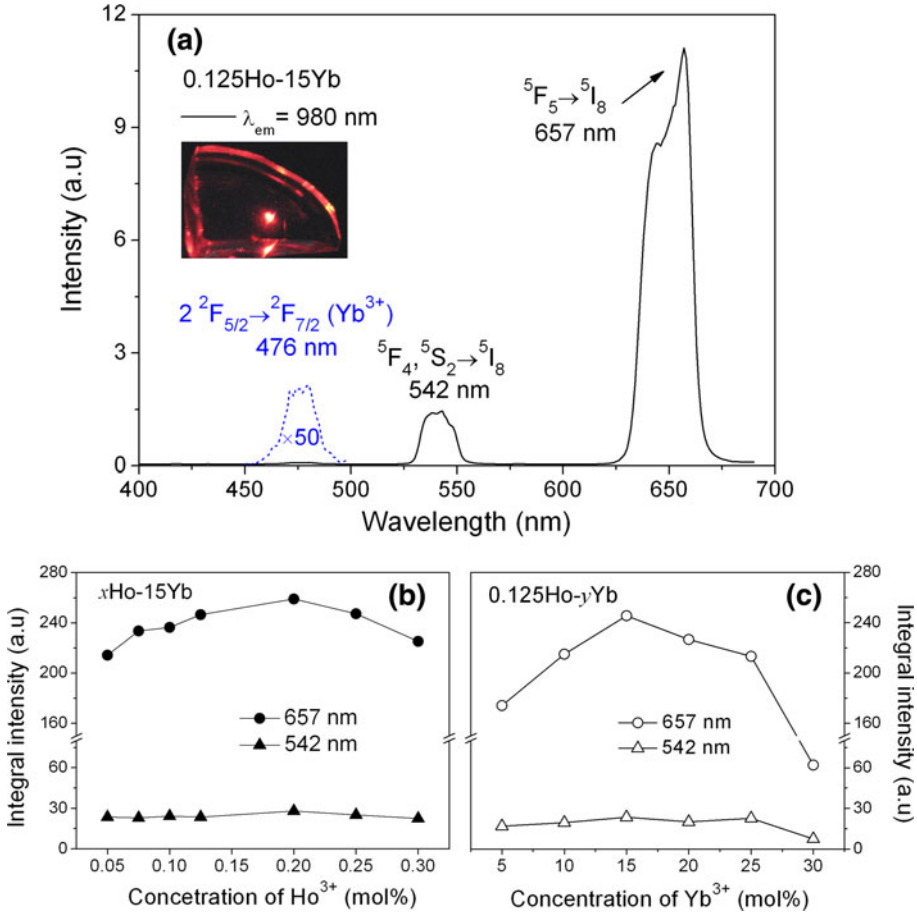

Fig. 6 **a** Visible upconversion emission spectrum and photograph of YBPF: 0.125Ho-15Yb under 980 nm laser excitation with the pump power about 450 mW/mm^2; **b** Dependence of the intensities of upconversion emissions on the concentration of Ho^{3+} and **c** that on the concentration of Yb^{3+}

emission is much stronger and I_{657nm}/I_{542nm} increases from about 9:1 to 13:1 as the concentration ratio of C_{Yb}^{3+}/C_{Ho}^{3+} decreases from 600:1 to about 16:1.

In frequency upconversion processes, the upconversion emission integral intensity I_{UP} will be proportion to the nth power of the pump power P_{ex}, i.e.,

$$I_{UP} \propto (P_{ex})^n, \quad (7)$$

where n is the number of pump photons required to excite the emitting state. Such plots for both the green ($^5F_4$, $^5S_2 \rightarrow {}^5I_8$) and red ($^5F_5 \rightarrow {}^5I_8$) emissions in YBPF: 0.05Ho-15Yb and YBPF: 0.5Ho-25Yb samples are presented in Fig. 7. The values of n obtained are all close to two, indicating that two-photon absorption processes are responsible for three upconversion emission bands. Due to a lower doping concentration of Ho^{3+}, no obvious inflections in these plots are observed, thus ruling out a photon avalanche upconversion mechanism [34, 35].

According to the concentration and pump-power dependences of the green and red upconversion emissions, the two-photon upconversion mechanisms for these emissions are briefly illustrated in Fig. 8. Firstly, Yb^{3+} ions are excited from the $^2F_{7/2}$ to $^2F_{5/2}$ level by absorbing laser photons due to their large absorption cross-section around 980 nm. Because the $^2F_{5/2}$ level of Yb^{3+} mismatches the $^5I_6$ level of Ho^{3+}, then ground Ho^{3+} is promoted to the $^5I_6$ levels by receiving a phonon-assisted transfer from Yb^{3+}. For the green emission, Ho^{3+} on the $^5I_6$ level is promoted to the $^5F_4$,$^5S_2$ levels directly by absorbing energy of laser photons (excited state absorption, *ESA*) or excited Yb^{3+} ions (energy transfer upconversion, *ET*). For the red emission, two possible upconversion channels are responsible for the population of the $^5F_5$ level: (I) The previously mentioned MPR from the $^5F_4$,$^5S_2$ to $^5F_5$ level. Apparently, this channel will result in a green-dominant upconversion light according to Fig. 3a. (II) The promotion from the $^5I_7$ level that populated via the MPR from the $^5I_6$ level. According to the discussion in Part 3.3, this $^5I_6 \rightarrow {}^5I_7$ relaxation is very fast, and thus makes the $^5I_7$ level efficiently populated after ground Ho^{3+} is excited. Meanwhile, the lifetime of the $^5I_7$ level is estimated to be about 3.0 ms, and it is long enough for the promotion to the $^5F_5$ level via ESA and/or ETU. In summary, in our upconversion case, the channel II is considered to be the major channel for the red upconversion emission. Moreover, this also will explain the much larger intensity ratio of I_{657nm}/I_{542nm} in the upconversion case, because the channel II generates only the red emission throughout whole upconversion process.

3.5 Temperature effect on the red-dominant upconversion light

Figure 9 and inset show the effects of temperature on the intensities of the green and red upconversion emissions in YBPF: 0.125Ho-15Yb ($P_{ex} \approx 150$ mW/mm^2). Due to the thermally enhanced non-radiative relaxations on all the excited levels of Ho^{3+}, both the green and red emissions intensities decrease drastically as temperature increases$^-$. On the other hand, increasing temperature facilitates the $^5I_6 \rightarrow {}^5I_7$ and $^5S_2$, $^5F_4 \rightarrow {}^5F_5$ MPRs, and then augments the intensity ratio of I_{657nm}/I_{542nm} from about 6:1 to 18:1 as Fig. 10 shows. This increment on the intensity ratio in

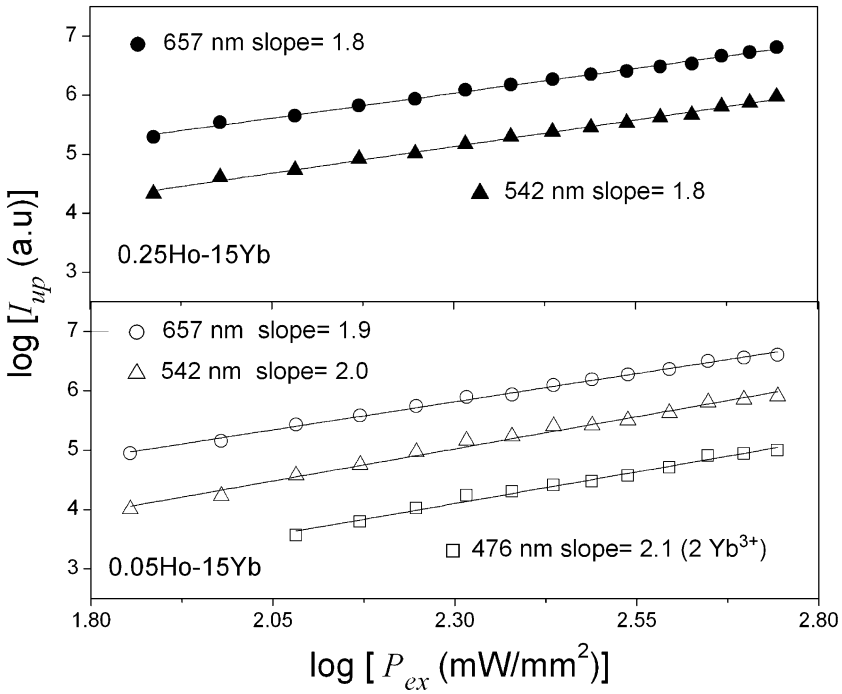

Fig. 7 Dependence of upconversion emission intensities on excitation power of 980 nm laser for YBPF:0.25Ho-15Yb and 0.05Ho-15Yb glasses at room temperature

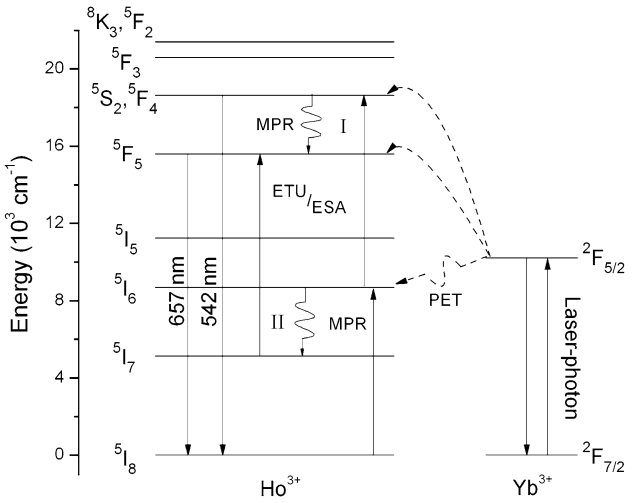

Fig. 8 Simplified energy-level diagram of Ho^{3+} and Yb^{3+} ions and upconversion luminescence mechanism for our samples. *Solid straight lines* with *upward* and *down arrows* denote pumping and upconversion transitions, and radiation transitions; *dot lines* denote energy transfer; *MPR, ESA, ETU* and *PET* are the acronyms for the multi-phonon-assisted relaxation, excited state absorption, energy transfer upconversion and phonon-assisted energy transfer, respectively

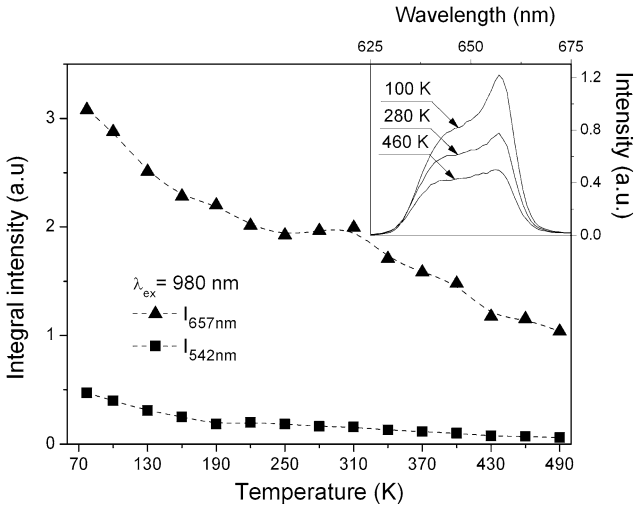

Fig. 9 Temperature effects on the intensities of the red and green upconversion emissions for YBPF:0.125Ho-15Yb sample (Inset: Temperature effect on the spectra shape of the red upconversion emission of Ho^{3+})

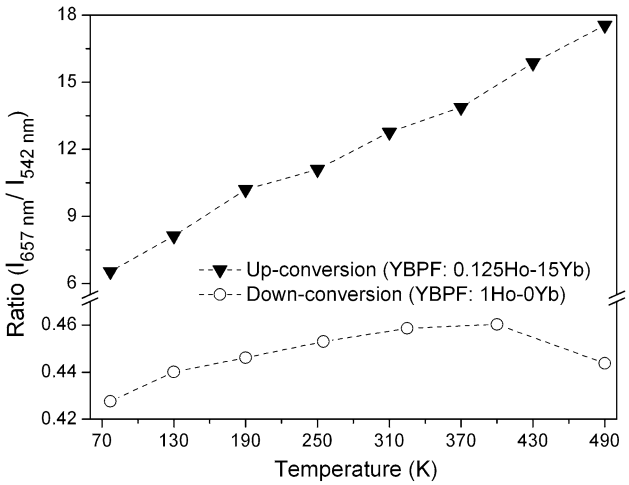

Fig. 10 Temperature effects on the intensity ratios of the red emission to the green one (I_{657nm}/I_{542nm}) in up- and down-conversion cases

the upconversion case is much greater than that in down-conversion case, further confirming that the bright red upconversion is mainly decided by the MPR relaxation on the $^5I_6$ level. Moreover, this increment is also greater than that induced by the concentration variations of Ho^{3+} and/or Yb^{3+}, indicating the red-dominant light of samples is mainly decided by the proper phonon energy of the host but not the doping concentrations of RE^{3+} ions.

Increasing temperature also affects the spectrum shape of the red emission. Upconversion spectra in Fig. 9 inset show that the ratio of the signal intensity at 643 nm to that at 657 nm increases from about 0.60–0.84 as temperature increases from 100 to 460 K. This ~643 (657) nm upconversion signal that can be ascribed to the $^5F_5 \rightarrow {}^5I_8$ transitions starting from the higher (lower) crystal-field components of the $^5F_5$ level and ending at lower (higher) crystal-field components of the $^5I_8$ level. And because the energy difference between each components in the $^5F_5$ and $^5I_8$ states are very small (a few kT), the higher crystal field components of the $^5F_5$ levels can be populated from the lower ones through the thermal agitation. Furthermore, the full width at half maximum (FWHM) increases from about 21.3 to 25.2 nm as temperature increases, and this can be related to the thermally enhanced electron–phonon interaction [36, 37].

4 Conclusions

Ho^{3+} singly doped and Ho^{3+}/Yb^{3+} co-doped YBPF glasses were fabricated and characterized. The experimental intensity parameters $\Omega_{2,\ 4,\ 6}$, spontaneous radiative transition probability and radiative decay time were calculated using Judd–Ofelt theory. The temperature dependence of relaxation rate of the $^5S_2$, $^5F_4 \rightarrow {}^5F_5$ was studied and the result revealed the $^5S_2$, $^5F_4 \rightarrow {}^5F_5$ relaxation was a 3-phonon-assisted process. For all Ho^{3+}/Yb^{3+} co-doped samples excited by a 980 nm CW LD at room temperature, a weak green emission peaking at 542 nm and a strong red emission peaking at 657 nm were recorded. This strong red emission could be interesting for its applications on the biomedical labels and color display. Power-dependent studies revealed that both green and red emissions of the samples result from 2-photon absorption processes. All the

results showed the bright red-dominant upconversion light of YBPF: Ho^{3+}/Yb^{3+} were decided by proper phonon energy of the samples: (1) The fast phonon-assisted relaxation from the $^5I_6$ level was favorable to the population on the $^5I_7$ level. (2) The lifetime of $^5I_7$ level is long enough to receive energy for the promotion to the $^5F_5$ level, from where the bright red emission originates.

Acknowledgments This work was supported by the National Nature Science Foundation of China (20971130, 20501023), the project of the combination of Industry and Research by the Ministry of Education and Guangdong Province (2008B090500027), and the Nature Science Foundation of Guangdong (5300527) and the Science and Technology Project of Guangzhou (2005Z2-D0061).

References

1. S.A. Wade, S.F. Collins, G.W. Baxter, J Appl Phys **8**, 4743 ((2003))
2. F. Vetrone, R. Naccache, V. Mahalingam, C.G. Morgan, J.A. Capobianco, Adv Funct Mater **19**, 2924–2929 (2009)
3. N.K. Giri, D.K. Rai, S.B. Rai, J. Appl Phys. **104**, 113107 (2008)
4. J. Yang, C. Zhang, C. Peng, C. Li, L. Wang, R. Chai, J. Lin, Chem Eur J **15**, 4649 (2009)
5. F.X. Gan, Optical Glass, Bejing Science Press 301 (1985)
6. L. Feng, J. Wang, Q. Tang, L. Liang, H. Liang, Q. Su, J Lumin **124**, 187 (2007)
7. L. Feng, Q. Su, Y. Li, C. Zheng, C. Wang, H. Du, Spectrochim Acta Part A **73**, 41 (2009)
8. W. Xiong, P. Yang, J. Liao, S. Lin, J Cryst Growth **280**, 212 (2005)
9. H. Wang, C. Tu, Z. You, F. Yang, Y. Wei, Y. Wang, J. Li, Z. Zhu, G. Jia, X. Lu, Appl Phys B **88**, 57 (2007)
10. N.M. Sangeetha, F.C.J.M. van Veggel, J Phys Chem C **113**, 14702 (2009)
11. B. Karmakar, P. Kundu, R.N. Dwivedi, J Non-Crystal Solids **289**, 155 (2001)
12. R. Lebullenger, L.A.O. Nunes, A.C. Hernandes, J Non-Crystal Solids **284**, 55 (2001)
13. A.M. Efimov, J Non-Crystal Solids **209**, 209 (1997)
14. M.S. Liao, Y.Z. Fang, H.T. Sun, L.L. Hu, Opt Mater **29**, 867 (2007)
15. L. Zhang, L. Wen, J. Zhang, L. Hu, Mater Chem Phys **91**, 166 (2005)
16. W.T. Carnall, P.R. Fields, K. Rajnak, J Chem Phys **49**, 4424 (1968)
17. M.J. Weber, J Non-Crystal Solids **74**, 167 (1985)
18. C.K. Jørgensen, B.R. Judd, Mol Phys **8**, 281 (1964)
19. S. Tananbe, T. Ohyagi, N. Soga, T. Hanada, Phys Rev B **46**, 3306 (1992)
20. S. Tanabe, T. Ohyagi, S. Todoroki, T. Hanada, N. Soga, J Appl Phys **73**, 8451 (1993)
21. H. Ebendor-Heidepriem, D. Ehrt, M. Bettinelli, A. Speghini, J Non-Crystal Solids **240**, 66 (1998)
22. Q. Su, Q.Y. Wang, S.X. Wu, Chin Chinese J Lasers **166**, 12 (1989)
23. B. Peng, T. Izumitani, Opt Mater **4**, 797 (1995)
24. K. Tanimura, M.D. Shinn, W.A. Sibley, Phys Rev B **30**, 2429 (1984)
25. R. Van Deun, K. Binnemans, C. Görller-Walrand, J.L. Adam, J Alloys Compd **283**, 59 (1999)
26. T. Suhasini, B.C. Jamalaiah, T. Chengaiah, J. Suresh Kumar, L. Rama Moorthy, Physica B **407**, 523 (2012)
27. D. Kasprowicz, M.G. Brib, A. Majchrowski, E. Michalski, A. Biadasz, J Alloys Compd **509**, 1430 (2011)
28. E.D. Reed Jr, H.W. Moors, Phys Rev B **8**, 980 (1973)
29. W.D. Partlow, H.W. Moos, Phys Rev **157**, 252 (1967)
30. L.A. Riseberg, H.W. Moos, Phys Rev **174**, 429 (1968)
31. M.J. Weber, Phys Rev B **8**, 54 (1973)
32. C.B. Layne, W.H. Lowdermild, M.J. Weber, Phys Rev B **16**, 10 (1977)
33. F. Auzel, D. Meichenin, F. Pellé, P. Goldner, Opt Mater **4**, 35 (1994)
34. F. Lahoz, I.R. Martín, J.M. Calvilla-Quintero, Appl Phys Lett **86**, 051106 (2005)
35. V. Lavín, F. Lahoz, I.R. Martín, U.R. Rodríguez-Mendoza, J.M. Cáceres, Opt Mater **27**, 1754 (2005)
36. M. Sendova-Vassileva, M. Iliev, A.V. Chadwick, J Phys Condens Matter **3**, 5407 (1991)
37. G. K. Liu; Spectroscopic Properties of Rare Earths in Optical Materials (Springer, Berlin, 2005)